LASER & PHOTONICS REVIEWS

REPRINT

Abstract: Plasmonic focusing with metallic probes has attracted extensive studies due to its successful applications in advanced technologies such as near-field scanning optical microscopy and tip-enhanced Raman spectroscopy. Here the fabrication and characterization of a unique spiral metallic taper with polarization-insensitive three-dimensional (3D) plasmonic focusing properties are reported. Metallic probes with spiral corrugations are readily fabricated along the surfaces of the conical structures with a 3D direct laser writing method followed by a metal deposition process. With the broken structural symmetry induced by the spiral corrugations, plasmonic focusing is demonstrated under excitation of linearly polarized light with different polarization directions. Moreover, apertures with various sizes can be flexibly introduced at the apex of the conical probe structures with direct fabrication, which enables the observation of scattered light from waveguide modes, cutoff of waveguide modes and scattering from surfaces plasmons, respectively. The studies provide a novel methodology of design, realization, and application of 3D plasmonic focusing structures.
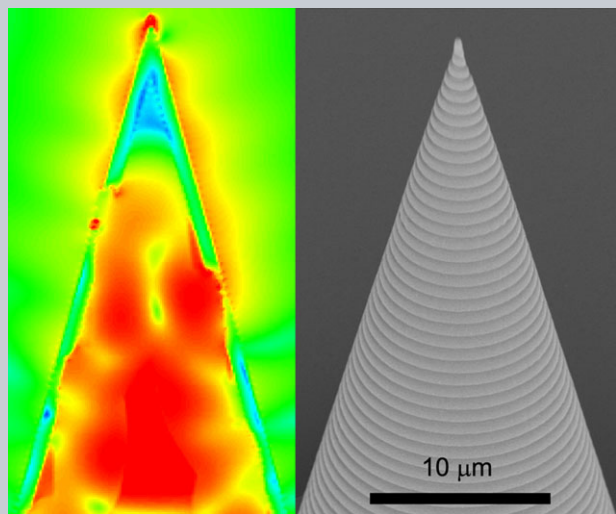
Direct laser writing of symmetry-broken spiral tapers for polarization-insensitive three-dimensional plasmonic focusing

Jiafang Li*,, Jiajia Mu**, Benli Wang, Wei Ding, Ju Liu, Honglian Guo, Wuxia Li, Changzhi Gu, and Zhi-Yuan Li***

1. Introduction

Surface plasmon polaritons (SPPs), which are electromagnetic waves confined at the metal-dielectric interface, intrinsically carry information and energy at nanoscale without suffering from the diffraction limits of light [1]. Manipulations of SPPs are therefore the essential tasks of many nano-optical devices which have been widely employed in biochemical sensings [2], nano-fabrications [3, 4], sub-diffraction-limit imagings [5], enhanced light-matter interactions [6], etc. Usually, when a p-polarized light illuminates a noble metal plane, intentionally designed structures like gratings, prisms, trenches, holes, slits, etc.[1] can help to excite SPPs. With proper choice of geometrical parameters, the excited SPPs can be subject to dispersion, interference, collimation, or focusing for versatile functionalities [2, 7–13].

Plasmonic focusing with metallic probes has attracted extensive studies due to their successful applications in sophisticated technologies such as near-field scanning optical microscopy (NSOM) [14] and tip-enhanced Raman spec-

troscopy [15]. In these applications, conical tapers with angle of few degrees are widely employed, with apertureless apex or nanoscale apertures on the apex. Light can be launched either from the bottom part of the tapers (named as internal illumination) [14, 16] or from the outside of the tapers (named as external illumination) [15]. The internal illumination usually requires radially polarized illumination other than linearly polarized excitation [16, 17]. This is because when excited by linearly polarized light, the SPPs on the outer surface of the metallic probes interfere destructively as they travel toward the tip due to the opposite polarities on the opposite sides of the symmetric tip [17]. The external excitation method, on the other hand, bypasses this requirement but greatly decreases the energy transfer efficiency (less than 1 part in 10^5 of the excitation energy is typically transferred to the tip apex) and increases the background noises. Although researchers have introduced coupling elements such as nanoscale gratings [18] on one side of the tapers apart from the apex, the complexity in fabrication and alignment limits their applications. To resolve these problems, pyramid-shape probes have recently

been examined in the context of three-dimensional (3D) plasmonic focusing [19]. The introduction of asymmetric nano-gratings or corrugations has been demonstrated on the surface of the pyramids for efficient focusing [19,20]. However, in this scheme, high efficiency requires strict alignment between the linearly polarized light and the asymmetric pyramid itself, which could be challenging in practical applications [21]. Therefore, low-noise 3D plasmonic focusing for polarization-insensitive excitation is highly desirable.

Recently, Lotito et al. numerically proposed a metal-coated probe with few semicircular spiral corrugations on the outer surface for superfocusing under arbitrarily-oriented linearly-polarized excitation [21]. However, this design has not been experimentally demonstrated so far because the state-of-the-art nanofabrication technologies such as electrochemical etching, electron-beam lithography (EBL) and focused ion beam (FIB) milling are not suitable to manufacture such a 3D structure. In this article, we propose a reproducible design of spiral conical structures for polarization-insensitive 3D plasmonic focusing. The designs are readily demonstrated by using metal deposition and a direct laser writing (DLW) [22,23] method that has the capability of fabricating sub-10-nm features [24]. Through fabricating spiral corrugations along the conical structures, direction-free asymmetries are introduced and polarization-insensitive plasmonic focusing is realized, which eliminates the complexity of both beam and polarization alignment. We also show that variable apertures can be introduced on the top of the conical structures by simple designs without supplementary fabrications. The demonstrated fabrications in this article represent an essential step toward the realization of practically usable and versatile micro-/nano-tips and apertures and in a broader aspect hold the potentials for versatile designs and applications of 3D plasmonic structures.

2. Experimental

2.1. Sample fabrications

The DLW we use in fabrication is based on two-photon polymerization (2PP) technique [22, 23] employed by a commercial fabrication system (Photonic Professional, *Nanoscribe GmbH*). In fabrication, a 780 nm femtosecond laser beam (with pulse width ∼120 fs and repetition rate ∼80 MHz) is focused into a negative photoresist (IP-L, *Nanoscribe GmbH*) by a high numerical aperture (NA) oil-immersion objective (100×, NA = 1.4, *Zeiss*). The polymerized elliptical voxel, as the replica of the laser focus after polymerization, is about 360 nm in width and 1000 nm in height, which ensures the overlap of the neighboring voxels for dr up to 210 nm. For smooth conical tapers and conical tapers with concentric corrugations, the laser focus is scanned layer-by-layer with circular routes in each layer, while between neighboring layers, the height is increased by dz and the radius is decreased by dr

($dz/dr = 4$). For spiral tapers, the laser focus is scanned with circular routes in which the radius decreases gradually with the increased height. To fabricate hollow conical structures, a hollow square frame is fabricated as the basis, whose width, height, and thickness are 21, 10, and 4 μm, respectively, with a hole of $4\times4\times6$ μm^3 in each side. After laser exposure, the sample is developed in 2-propanol for one hour for fully development. After the DLW process, a 70-nm-thick gold (or silver) film is deposited onto the structures through magnetron sputtering.

2.2. FDTD simulations

The 3D finite-difference time-domain (FDTD) method is used for the calculation of electric fields. The source is set as x-polarized, y-polarized or circularly polarized, respectively in the calculation. Perfectly matched layers (PML) are added along all-directions. Due to the asymmetry of the model, the grid size is set as 10 nm to reduce the computation cost. The vertex angle of conical structures is kept as 14 degrees, and the thickness of gold (or silver) is 70 nm. The dielectric constant data of gold (or silver) are taken from Ref. [25].

2.3. Characterizations

For SEM characterizations, the samples are coated with 70-nm silver and characterized with a SEM equipped in an electron-beam lithography system (Raith 150). For white light illumination, the conical structures are illuminated by the tungsten lamp from the bottom part of the cone. A filter set is inserted to confine the incident light in the wavelength range from 650 to 750 nm. The images of the excited samples are measured with an inverted microscope (Leica, DMIRB) equipped with a CCD camera. For coherent excitation, a Ti-sapphire laser is employed with wavelength of 794 nm, pulse width of 70 fs, and repetition rate of 73 MHz. The laser beam is focused by a 10× objective with NA = 0.3 and the signals are collected by a 100× objective with NA = 0.9. After filtered by a short pass filter (Semrock, OD$_{avg}$ > 8 within 680–1040 nm), the spectra are collected by an optical fiber and measured by a spectrometer (Ocean Optics, QE65000).

3. Results and discussions

The proposed designs are shown in Fig. 1, where a gold-coated hollow conical taper is firstly introduced for comparisons. As shown in Fig. 1a, the taper angle is chosen at 28°, whose numerical aperture is matched with that of single mode fibers (the taper angle can be varied to have different spectral response). This conical taper can be regarded as a tapered cylindrical waveguides supporting different kinds of local waveguide modes (WGMs) [16, 21]. As the radius of the taper decreases, all these WGMs gradually run into
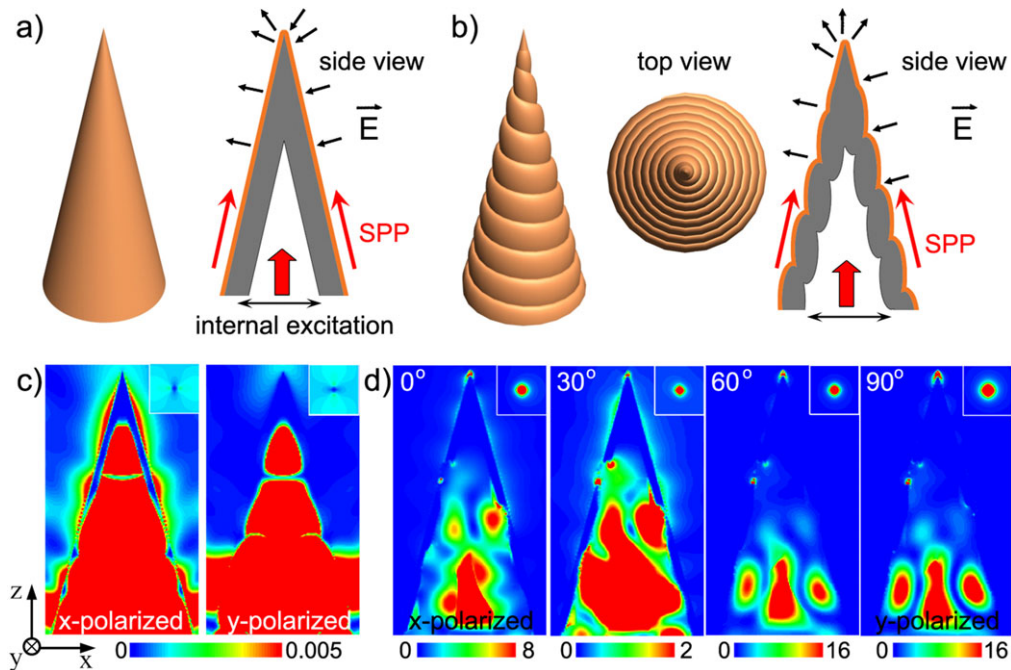
Figure 1 Schematic view and side view of **(a)** a hollow conical taper (named conical taper) and **(b)** a taper with spiral corrugations along the conical surface (named spiral taper). The tapers have a height of h, a bottom radius of r ($h/r = 4$), a dielectric layer (gray area) with thickness of $t_1 = 360$ nm and refractive index of 1.52, and a metal layer (orange area) with thickness of $t_2 = 70$ nm. The corrugation period of the spiral taper is dg. **(c)** Simulated E-field intensity distribution in the x-z plane for the gold-coated conical taper in **(a)** under internal excitation with x-polarized and y-polarized light, respectively, at wavelength of 800 nm. The E-field intensity distribution in the x-y plane 10 nm above the tip is shown in the **Inset**, indicating no focusing effects. **(d)** Simulated E-field intensity distribution in the x-z plane for the gold-coated spiral taper in **(b)** under internal excitation with light of different polarizations at wavelength of 800 nm. 0° corresponds to x-polarized excitation while 90° corresponds to y-polarized excitation. The E-field intensity distributions in the x-y plane 10 nm above the tip are shown in corresponding **Insets**, which show focusing effect irrespective to the excitation polarization. Image sizes of **(c–e)**: 1.4×2.7 μm^2. Image sizes of the **Inset**: 200×200 nm^2.

cutoff so that no WGMs can carry energy into the apex of the taper. However, at some specific radii of the taper where the wave vectors of some WGMs match with the wave vector of the SPP on the outer surface between the metal and the air, the WGMs transmit part of energy to this outer SPP mode, which then continuously implements the energy concentration towards the taper apex [16]. However, when the structure is internally illuminated by linearly polarized light, due to the symmetry of the structures, the electric field (E-field) of the excited SPPs have opposite polarities on the opposite sides of the taper, which cancel out each other when SPPs arrive at the apex (Fig. 1a) [17, 21]. This can be clearly seen in our finite-difference time-domain (FDTD) simulation results in Fig. 1c, where the E-field intensity distributions do not show any focused spot around the apex under excitation with different polarizations.

The key to overcome the above issue is to introduce asymmetric elements like nanogratings or corrugations on the outer surface of the tapers which are able to offset the propagation phase of the coupled SPPs on the opposite sides of the taper so that SPPs can interfere constructively at the apex [26]. Based on this principle and considering the feasibility in fabrication, we design a symmetry-broken

spiral conical structure (named spiral taper in the following studies). As shown in Fig. 1b, the spiral taper is composed of a hollow polymer template that can be fabricated with DLW and a thin layer of metals coated at the outer surface. There are three important ingredients in our model design. Firstly, we choose a noble metal layer (gold or silver) with thickness of 70 nm, which is thick enough to efficiently block the background noise arising from the internal illumination. Secondly, the hollow nature of the tapers reserves the advantages such as high power throughput, high thermal threshold and low pulse chirping effects [27]. Most importantly, the spiral corrugation is adopted mainly because this type of corrugation can be readily produced on the surfaces of the structures by using the well-controlled DLW method (see *Experimental* and following descriptions).

Based on such a design, a gold-coated spiral taper with the corrugation period of 782 nm is modeled with FDTD method (the corrugation period matches the SPP wavelength at the gold/air interface with dielectric constant of gold $\varepsilon_{Au} = -22.918 + 0.814i$ at light wavelength of 800 nm) [25]. Figure 1d shows the simulated E-field intensity distributions in the same x-z planes but under linearly polarized excitation at various polarization directions. One can see
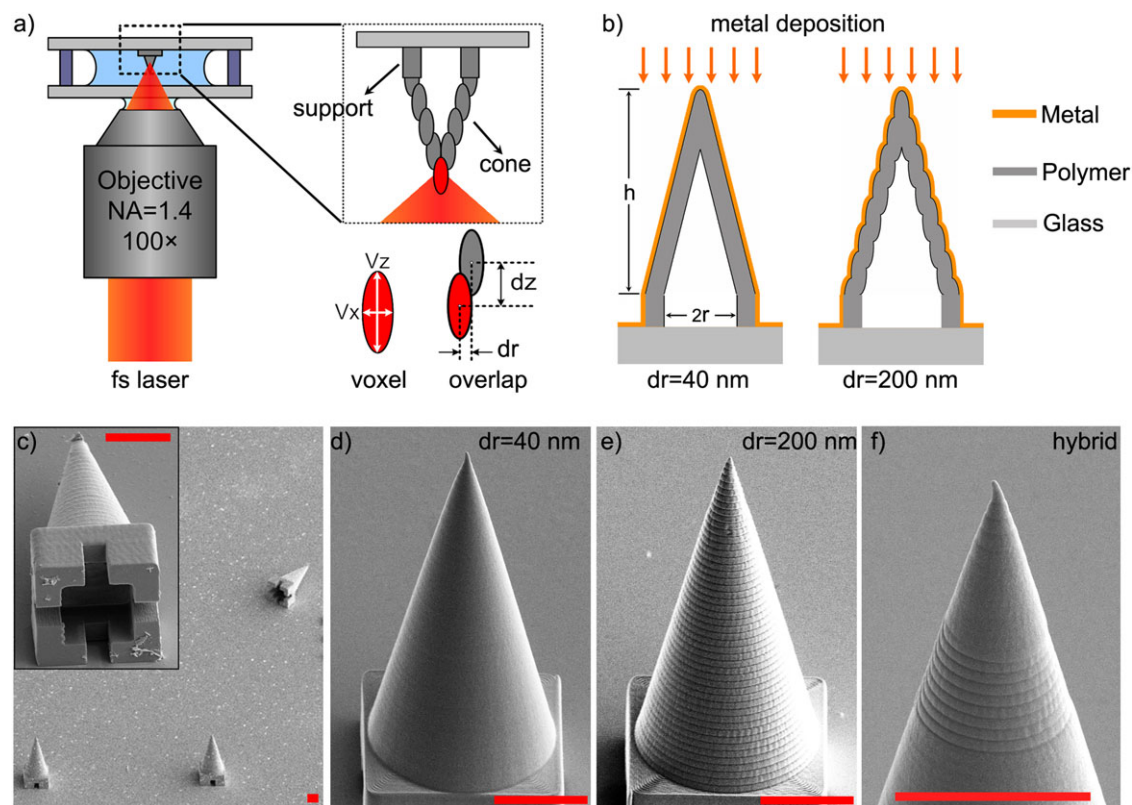
Figure 2 **(a)** Schematic diagram for DLW of hollow conical structures. The side view of the scanning scheme is shown in the right side, where the replica of the laser focus, named as voxel, is scanned layer-by-layer. To form the conical shape, the position of the voxels between adjacent layers is shifted laterally by dz and axially by dr. **(b)** After DLW, the polymerized structures are deposited with metals. A larger dr results in corrugations along the surfaces of the conical structures. **(c–f)** SEM images of fabricated structures with $h = 40$ μm and $2r = 20$ μm. All scale bars: 10 μm. **(c)** shows the overall layout of the structures and the designed support in the **Inset** enables the fabrication of hollow conical structures. **(d)** and **(e)** show conical structures fabricated with $dr = 40$ and 200 nm, respectively. **(f)** is a hybrid design which shows periodical corrugations 10 μm apart from the apex of the taper on smooth surface.

that a focus spot is clearly shown in all cases, indicating that the spiral taper can be used for plasmonic focusing of linearly polarized light and the focusing occurs independently on the excitation polarization direction. It should be noted that the E-field intensity at the apex is enhanced by more than three orders of magnitude compared with conical tapers without spiral corrugations. This indicates that the spiral corrugations are not only helpful for focusing SPPs towards the apex but also favorable for the energy transfer from WGMs to SPPs due to the extra momentum provided by the periodical corrugations.

To experimentally realize such a design, we employ the DLW method based on 2PP technique [22, 23] with a commercial fabrication system [28] (see Experimental), as schematically shown in Fig. 2a. Due to the 3D point-by-point fabrication nature of DLW, arbitrary 3D structures can be fabricated by scanning the focused laser spot inside the photoresist with programmed routes. However, to achieve a very thin layer of conical template in large scale is still challenging because a slight weakness in mechanical strength could result in the collapse of the structures. We overcome this issue by designing a single scanning process, with which the fabricated hollow conical templates exhibit

strong mechanical properties with sidewall thickness less than 400 nm and taper height around 40 μm. As schematically plotted in Fig. 2a, the conical structures are designed by shifting the position of the polymerized focal regions (named as voxels) in adjacent layers laterally by dz and axially by dr while keeping them connected. This offset results in the conical shape of the fabricated structure and simultaneously induces corrugations on the polymer structures, which will be finally transfered to the outer metallic layer after metal deposition (Fig. 2b). In order to obtain proper parameters to realize spiral tapers, we first study the conical structures formed with concentric circular corrugations with decreased radius towards the apex. As shown in Fig. 2b, with a fixed ratio of $dz/dr = 4$, a large $dr = 200$ nm results in periodical circular corrugations along the surface of the conical structures while a small $dr = 40$ nm results in conical taper with smooth surface. To experimentally fabricate such a hollow conical structure, a hollow square support is fabricated below the conical structure (Fig. 2c), with the help of which the unpolymerized photoresist inside the cones can be washed away during the development of the structures (see *Experimental*). As shown in Fig. 2d, when $dr = 40$ nm, a conical taper with smooth surface
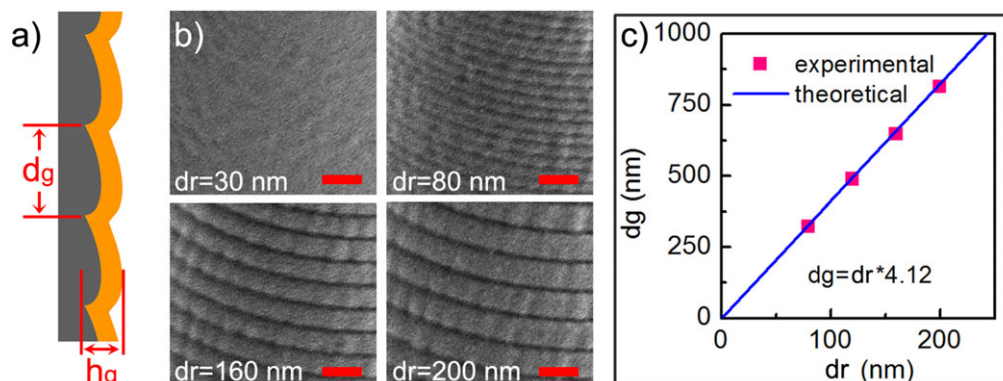
Figure 3 **(a)** Schematic illustration of the periodical corrugations on the conical surface with a periodicity of *dg* and modulation depth of *hg*. **(b)** SEM images of fabricated circular corrugations on conical surfaces with different *dr* as noted. Scale bars: 1 μm. **(c)** Experimentally measured and theoretically designed *dg* with relation of *dr*.

is obtained. In comparisons, when $dr = 200$ nm, concentric circular corrugations are clearly observed at the outer surface of the structures (Fig. 2e). It should be mentioned that the fabrication parameters can be flexibly designed to form hybrid conical structures with corrugations at desired region, like the structure shown in Fig. 2f.

The geometry of the corrugations on metal film is schematically shown in Fig. 3a, where the corrugation period *dg* is highly dependent on the value of *dr*. To obtain the relationship between *dg* and *dr*, we fabricate conical structures with circular corrugations under different *dr* and measured the value of *dg* from scanning electron microscope (SEM) images (Fig. 3b). With our design of $dg = \sqrt{dz^2 + dr^2}$, one gets $dg = 4.12*dr$ when $dz/dr = 4$. As plotted in Fig. 3c, the measured data fits well with our theoretical design, which forms the basic rule for designing our conical structures with spiral corrugations.

The arbitrary 3D fabrication capability of the DLW method also allows us to fabricate conical structures with various apertures at the apexes by simply terminating the writing programs of the conical structures at certain height (as shown in Fig. 4a). This direct fabrication process can bypass the FIB milling and avoids any pollution accompanied by Ga^{3+} ion implantations. As shown in the SEM images in Figs. 4b–d, apertures with radius down to 120 nm are fabricated by "shortening" the top part of the normal conical tapers. By further optimizing the design parameters, the aperture radius can be decreased to less than 100 nm, holding the potentials for probe design of NSOM. Since the WGMs are cut off at certain radius of the taper [16], the easy fabrication of conical tapers with various apertures facilitates the indirect observations of the coupling from the WGMs to SPPs modes. As show in Figs. 4e–g, when conical structures with apertures of various radii are illuminated with unpolarized white light (wavelength region 650–750 nm), different "focusing patterns" are observed (here the focuses are determined at the position where the light spots are brightest and smallest). Figure 4e shows the case that when the aperture is very large, WGMs transmit through

the aperture and both light from WGMs and SPPs can be collected by the objective lens. When the radius of the aperture decreases to a critical value where the WGMs are nearly cut off, as recorded in Fig. 4f, the signals from the WGMs are diminished while the coupled SPPs are localized and strongly scattered by the boundary of the aperture. When the radius of the aperture continues to decrease, the WGMs are completely cut off and only the light from scattered SPPs is observed, as clearly seen in Fig. 4g. To mimic this observation, FDTD simulations with circularly polarized excitation are conducted at wavelength 700 nm. The results in Figs. 4h–j clearly show the evolution of E-field distribution from the WGMs, to the cutoff WGMs, and then to the SPP modes, respectively, which support the observation in Figs. 4e–g very well.

With the basis studied above, we finally obtain the optimized structure parameters for the fabrication of spiral tapers, which are $h = 40$ μm, $r = 10$ μm, $dr = 190$ nm, $dz = 760$ nm. With such parameters, a spiral taper with high quality is successfully fabricated with corrugation period of $dg = 783$ nm, as shown in Fig. 5a–c. It should be mentioned that although the parameters are fixed, the fabrication conditions including laser exposure power, scanning speed and scanning strategy are still very crucial. Nonuniform exposure that is caused by the delay time at mesh points and over-exposure at the connecting points could result in tapers with waved surfaces, as shown in the inset of Fig. 5b. The structures in Fig. 5a–c are fabricated by uniformly scanning the laser focus in a continuously programmed spiral routes and therefore show the best quality and uniformity among more than 50 samples. It should be mentioned that the curvature radius of the tip in Fig. 5b is about 125 nm, which could be technically improved to sub-10 nm with the more sophisticated hybrid DLW technique as in Ref. [24] but this is out of the scope of this article.

In order to demonstrate the improved focusing properties by the introduction of spiral corrugations, the fabricated conical taper and spiral taper are illuminated by a femtosecond laser with pulse duration of 70 fs and central
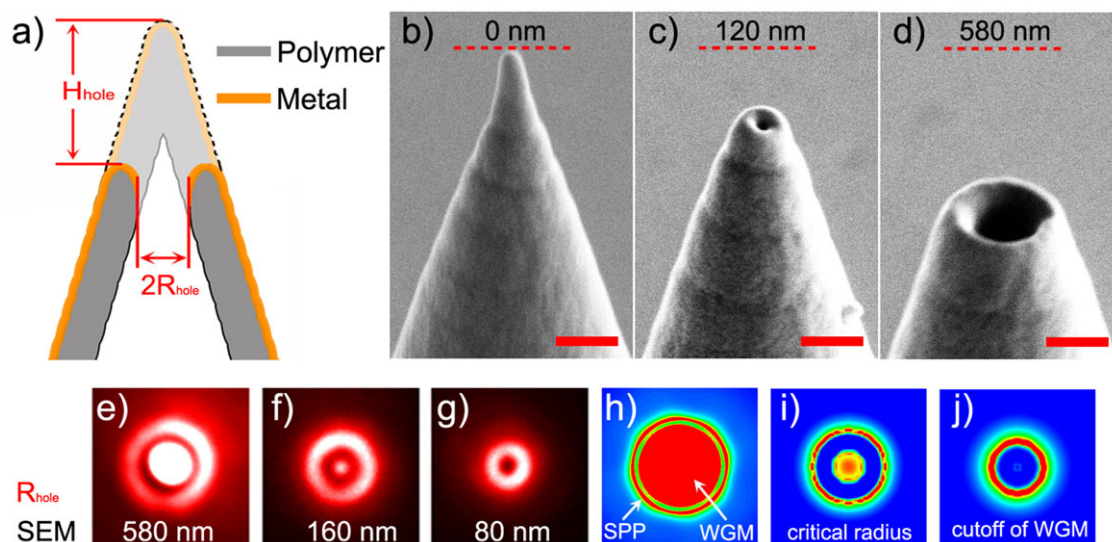
Figure 4 **(a)** Schematic diagram for DLW of hollow conical structures with an aperture on the top (with radius R_{hole}). **(b–d)** SEM images of 70-nm silver-coated structures with different R_{hole} as noted. Scale bars:1 μm. **(e–g)** False-color optical microscope images of the "focuses" of the fabricated structures (with different R_{hole} as noted) under internal excitation with unpolarized white light (wavelength region: 650–750 nm). The measured R_{hole} with SEM are shown at the bottom. Image sizes: 5×5 μm². **(h–j)** FDTD simulated E-field intensity distribution of conical structures at the top planes with aperture radius of 580, 120 and 80 nm, respectively. The E-field from WGMs and SPP modes are noted. From **h)** to **j)**, corresponding to figures from **e)** to **g)**, the bright areas are seen evolved from the transmitted WGMs to scattered SPPs.

wavelength of 794 nm (see *Experimental*). As shown in the optical microscopic images of Fig. 5d, the focus patterns of the conical taper are blurred when excited with linearly polarized light at varied polarization directions. In comparison, the recorded images from the spiral taper show a clean and bright focus spot irrespective of the polarization directions. To compare the light intensity of the focus spot and the background noise, the recorded images are dissected along parallel and perpendicular directions, respectively, crossing the focus spot. As shown in Fig. 5e, due to the anisotropic property of the background noise, the noise level can be obtained by comparing the two crosscut curves. In such a way, the relative intensity ratios between the peak intensity within the focus spot and the background noise outside the apex region are calculated, which are ∼3:1 and ∼6:1, respectively, for the conical taper and spiral taper. Although these images are recorded in far-field, the improvement in focusing under the same excitation condition ($P = 0.02$ μW) is obvious and consistent with the theoretical predictions. It should be mentioned that the observed improvements between the spiral taper and conical taper in Fig. 5d are not as much as that of the simulated results in Figs. 1c–d. This is caused by two reasons. First, far-field characterization cannot reflect the complete information of local field and the emission from coupled SPP outside the apex region can also be measured as background noise. Second, some of the fabricated conical tapers are not completely symmetric due to some fabrication imperfections such as the tilted tip observed in Fig. 2f. Such degradation in symmetry could induce some focusing effect [29] when the excitation polarization direction is parallel to

the tilting direction, as simulated in Fig. 5f. However, this asymmetry-induced focusing effect is sensitive to excitation polarization and no focusing effect is observed if the polarization direction is perpendicular to the tilting direction, as shown in Fig. 5f. Therefore, the polarization-insensitive focal spots of the spiral taper in Fig. 5d are uniquely benefited from the spiral corrugations.

Furthermore, it is well known that in the plasmonic focusing region, the local E-field intensity is greatly enhanced, which results in strong light-matter interactions and facilitates the generation of nonlinear optical phenomenon like high-order harmonic generations [30] and two-photon excitations [6]. Due to the strongly enhanced E-field at the apex of our conical tapers, clear nonlinear optical phenomenon is observed when the laser power is increased to 1 mW. As shown in Fig. 5g, both conical taper and spiral taper show visible photoluminescence under linearly polarized excitation, while the photoluminescence from the spiral taper is ∼30% stronger than that from the conical taper. After integrating the measured spectra and calibrating the collection efficiency, the integrated emission intensity shows a quadratic relationship with low pump power (<1 mW), as plotted in Fig. 5h. This clearly indicates two-photon photoluminescence of the structure, which gradually shows saturation effect when laser power is larger than 1 mW. Compared with the photoluminescence spectra from gold film in Ref. [31], the measured photoluminescence has a similar wavelength range from 420 to 660 nm (the longer wavelength part is influenced and damped by the laser filter) but a peak at shorter wavelength, the origin of which is interesting for further studies.
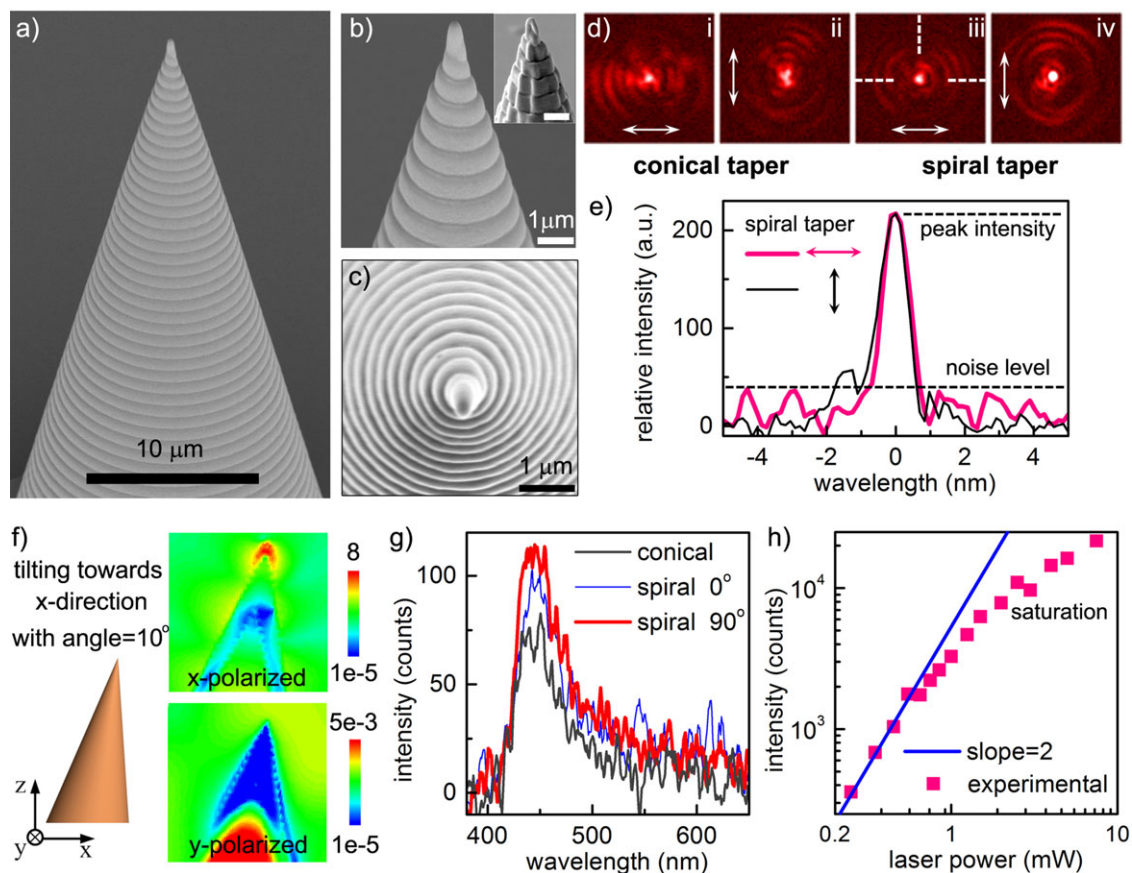
Figure 5 **(a–c)** Side-view and top-view SEM images of a fabricated spiral taper. The **Inset** of **(b)** shows a waved sample under improper fabrication condition. **(d)** False-color images of focus patterns of gold-coated conical taper and spiral taper under linearly polarized excitation with different polarization direction. Excitation wavelength: 794 nm. Image sizes: 12.5×12.5 μm^2. Laser power: 0.02 μW. **(e)** Crosscut intensity of the image in Fig. 5d-iii along parallel and perpendicular directions indicated by the dashed lines. **(f)** E-field intensity distributions (in log scale) in x-z planes with a conical taper tilted along x-direction with angle of 10°. Focusing effect appears and disappears when excitation polarization is parallel (x-polarized) and perpendicular (y-polarized) to the tilting direction, respectively. Image sizes: 0.8×0.8 μm^2. **(g)** Measured photoluminescence spectra of the conical taper and spiral taper under linearly polarized excitation with different polarization direction. Laser power: 1 mW. **(h)** Integrated spectral intensity as a function of pump power in log-log plot. The blue line with a slope of two is for a clear demonstration of the quadratic relationship under low pump intensities.

4. Conclusions

In conclusion, we have proposed and demonstrated a spiral conical structure that possesses polarization-insensitive 3D plasmonic focusing properties. Metallic hollow conical tapers with smooth surface, circular corrugations, and spiral corrugations have been successfully fabricated with the DLW method followed by a metal deposition process, which has shown great flexibility by fabricating various apertures at the taper tip. With the broken structural symmetry induced by the spiral corrugations, polarization-independent plasmonic focusing is aroused. Moreover, interesting two-photon photoluminescence has been demonstrated from the spiral taper under excitation with femtosecond laser, which shows 30% enhancement compared with that from the conical taper. As far as we know, the conical structures we demonstrated are unique since

they are reproducible and exceed the capability of traditional nanofabrication techniques like EBL and FIB. Furthermore, a fully metallic hollow conical probe could be achieved by removing the thin-layer polymer template [32]. In comparisons with solid probes, the hollow nature of the fabricated conical structures holds the potential advantages such as high power throughput and low pulse chirping. More importantly, since DLW has been demonstrated for fabrication of 3D structures on fiber tips [33], the proposed conical structures is capable of being integrated with fiber technology. Therefore, with the proposed principle and methodology, 3D plasmonic structures with versatile surface topographies, with or without apertures, can be realized to manipulate the wavefront of SPPs for desirable purposes [12, 13]. This could build up a novel platform for applications of 3D plasmonic focusing in areas such as near-field imagings, surface-enhanced Raman spectroscopy,

high-order harmonic generations, strong-field physics, etc. Considering that the cutting-edge fabrication resolution of DLW has nowadays been pushed to sub-10 nm level [24], further studies will be focused on improving the sharpness of the apex of fabricated structures, as well as exploring the nonlinear optical applications of the spiral tapers.

References

[1] W. L. Barnes, A. Dereux, and T. W. Ebbesen, Nature **424,** 824–830 (2003).

[2] S. Lal, S. Link, and N. J. Halas, Nature Photon. **1,** 641–648 (2007).

[3] Z. W. Liu, Q. H. Wei, and X. Zhang, Nano Lett. **5,** 957–961 (2005).

[4] W. Srituravanich, N. Fang, C. Sun, Q. Luo, and X. Zhang, Nano Lett. **4,** 1085–1088 (2004).

[5] N. Fang, H. Lee, C. Sun, and X. Zhang, Science **308,** 534–537 (2005).

[6] E. J. Sanchez, L. Novotny, and X. S. Xie, Phys. Rev. Lett. **82,** 4014–4017 (1999).

[7] H. J. Lezec, A. Degiron, E. Devaux, R. A. Linke, L. Martin-Moreno, F. J. Garcia-Vidal, and T. W. Ebbesen, Science **297,** 820–822 (2002).

[8] T. W. Ebbesen, H. J. Lezec, H. F. Ghaemi, T. Thio, and P. A. Wolff, Nature **391,** 667–669 (1998).

[9] X. G. Luo and T. Ishihara, Appl. Phys. Lett. **84,** 4780–4782 (2004).

[10] M. I. Stockman, Phys. Rev. Lett. **93** (2004).

[11] L. L. Yin, V. K. Vlasko-Vlasov, J. Pearson, J. M. Hiller, J. Hua, U. Welp, D. E. Brown, and C. W. Kimball, Nano Lett. **5,** 1399–1402 (2005).

[12] Y. H. Chen, L. Huang, L. Gan, and Z. Y. Li, Light-Sci. Appl. **1,** e26 (2012).

[13] Y. H. Chen, M. Q. Zhang, L. Gan, X. Y. Wu, L. Sun, J. Liu, J. Wang, and Z. Y. Li, Opt. Express **21,** 17558–17566 (2013).

[14] R. C. Dunn, Chem. Rev. **99,** 2891–2927 (1999).

[15] R. M. Stockle, Y. D. Suh, V. Deckert, and R. Zenobi, Chem. Phys. Lett. **318,** 131–136 (2000).

[16] W. Ding, S. Andrews, and S. Maier, Phys. Rev. A **75** (2007).

[17] A. Bouhelier, J. Jrenger, M. R. Beversluis, and L. Novotny, J. Microsc. **210,** 220–224 (2003).

[18] C. Ropers, C. C. Neacsu, T. Elsaesser, M. Albrecht, M. B. Raschke, and C. Lienau, Nano Lett. **7,** 2784–2788 (2007).

[19] N. C. Lindquist, P. Nagpal, A. Lesuffleur, D. J. Norris, and S. H. Oh, Nano Lett. **10,** 1369–1373 (2010).

[20] N. C. Lindquist, T. W. Johnson, P. Nagpal, D. J. Norris, and S. H. Oh, Sci. Rep. **3,** 1857 (2013).

[21] V. Lotito, U. Sennhauser, C. Hafner, and G. L. Bona, Plasmonics **6,** 327–336 (2011).

[22] S. Kawata, H. B. Sun, T. Tanaka, and K. Takada, Nature **412,** 697–698 (2001).

[23] B. Jia, J. Li, and M. Gu, Aust. J. Chem. **60,** 484–495 (2007).

[24] Z. S. Gan, Y. Y. Cao, R. A. Evans, and M. Gu, Nat. Commun. **4** (2013).

[25] M. J. Weber, Handbook of Optical Materials (CRC Press, 2002).

[26] L. Valeria, S. Urs, and C. Hafner, Opt. Express **18,** 8722–8734 (2010).

[27] Y. Y. Wang, Y. Y. Huang, and X. J. Zhang, Opt. Express **18,** 14004–14011 (2010).

[28] J. K. Gansel, M. Thiel, M. S. Rill, M. Decker, K. Bade, V. Saile, G. von Freymann, S. Linden, and M. Wegener, Science **325,** 1513–1515 (2009).

[29] T. N. Thi, K. Tanaka, M. Tanaka, and D. N. Chien, J. Opt. Soc. Am. A **30,** 1113 (2013).

[30] I. Y. Park, S. Kim, J. Choi, D. H. Lee, Y. J. Kim, M. F. Kling, M. I. Stockman, and S. W. Kim, Nature Photon. **5,** 678–682 (2011).

[31] M. R. Beversluis, A. Bouhelier, and L. Novotny, Phys. Rev. B **68** 115433 (2003).

[32] N. Tetreault, G. von Freymann, M. Deubel, M. Hermatschweiler, F. Perez-Willard, S. John, M. Wegener, and G. A. Ozin, Adv. Mater. **18,** 457–460 (2006).

[33] H. E. Williams, D. J. Freppon, S. M. Kuebler, R. C. Rumpf, and M. A. Melino, Opt. Express **19,** 22910–22922 (2011).